

The International Journal of Robotics Research

<http://ijr.sagepub.com/>

Contact Detection in Microrobotic Manipulation

W.H. Wang, X.Y. Liu and Y. Sun

The International Journal of Robotics Research 2007 26: 821

DOI: 10.1177/0278364907080254

The online version of this article can be found at:

<http://ijr.sagepub.com/content/26/8/821>

Published by:



<http://www.sagepublications.com>

On behalf of:



[Multimedia Archives](#)

Additional services and information for *The International Journal of Robotics Research* can be found at:

Email Alerts: <http://ijr.sagepub.com/cgi/alerts>

Subscriptions: <http://ijr.sagepub.com/subscriptions>

Reprints: <http://www.sagepub.com/journalsReprints.nav>

Permissions: <http://www.sagepub.com/journalsPermissions.nav>

Citations: <http://ijr.sagepub.com/content/26/8/821.refs.html>

W. H. Wang
X. Y. Liu
Y. Sun

Advanced Micro and Nanosystems Laboratory
University of Toronto, Canada
sun@mie.utoronto.ca

Abstract

This paper presents a computer vision-based method for visually detecting the contact between an end-effector and a target surface under an optical microscope during microrobotic manipulation. Without using proximity or force/touch sensors, this method provides a submicrometer detection accuracy and possesses robustness. Fundamentally, after the establishment of contact in the world frame, further vertical motion of the end-effector (flexible or stiff) induces horizontal motion in the image plane. Contact between a micropipette tip and a glass slide in the scenario of microrobotic cell manipulation is used as an example to elaborate on the detection method. Experimental results demonstrate that the computer vision-based method is capable of achieving contact detection between the micropipette and the glass slide surface with an accuracy of $0.2\ \mu\text{m}$. Furthermore, 1000 experimental trials reveal that the presented method is robust to variations in illumination intensity, microscopy magnification, and microrobot motion speed.

KEY WORDS—microrobotic manipulation, contact detection, computer vision microscopy

1. Introduction

Autonomous and tele-operated manipulation of micrometer sized objects is essential in both biological/engineering research and for the commercial success of many microscaled technologies (Junno et al. 1995; Ramachandran 1998; Vikramaditya and Nelson 1999; Lee et al. 2004). In microrobotic manipulation, an end-effector, such as a MEMS (microelectromechanical systems) based microgripper, microprobe, or a glass micropipette controlled by a microrobot is used to interact with micro-objects under an optical microscope (Sun and

Contact Detection in Microrobotic Manipulation

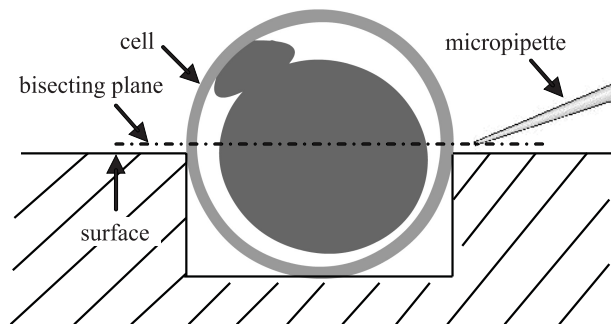


Fig. 1. The micropipette tip requires being located in the bisecting plane for interacting with the object (e.g., biological cell) along the centerline during microrobotic manipulation.

Nelson 2002). An important operation in micromanipulation is the precise determination of the relative vertical positions of the end-effector and the micro-object to be manipulated.

The schematic in Figure 1 shows the side view of a biological cell held in a patterned cavity for such tasks as microrobotic cell manipulation or single cell mechanics studies, in which the micropipette is required to push/penetrate the cell along the centerline of the cell. To position the micropipette in the desired bisecting plane (Figure 1), the relative vertical positions of the micropipette tip and the device surface must be precisely determined. Without loss of generality, detection of the contact between a micropipette tip and a substrate surface is taken as an example in this paper to illustrate the presented technique.

Existing methods employ proximity sensors (Li 1996; Haitjema et al. 2001; Trummer et al. 2004), piezoresistive sensors (Hatzivasiliou and Tzafestas 1994; Sitti and Hashimoto 2000), or piezoelectric touch sensors (Fukuda et al. 1998; Kanda et al. 1999; Arai et al. 2003; Shen et al. 2004) to determine the relative vertical coordinates between the end-effector and the target surface. The integration of sensors with end-effectors is often difficult (e.g., using epoxy) and complicates system setup. As contact-type sensors at the microNewton levels are fragile and prone to damage, extra care must be taken in sen-

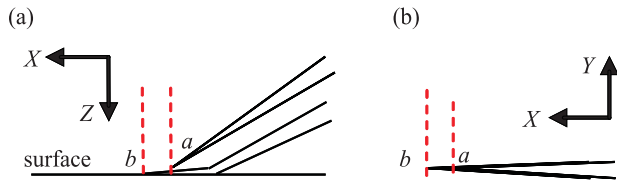


Fig. 2. Tip and surface in the world frame. (a) Side view. (b) Top view.

sor overloading protection. Furthermore, reported contact detection resolutions using additional sensors are often limited to several microns, calling for methods capable of providing a better detection resolution without using additional sensors.

As microrobotic cell manipulation and the assembly of microsystems are universally conducted under an optical microscope that provides high-resolution, low depth-of-field visual feedback, it is highly desirable to utilize microscopy visual feedback for contact detection. Assuming that the micropipette tip and the target (e.g., glass slide surface) share the same focal plane, autofocusing algorithms (Subbarao and Tyan 1998; Geusebroek et al. 2000; Sun et al. 2004) can be used to independently servo the micropipette tip and the glass slide surface to bring them to a co-plane.

However, autofocusing algorithms are sensitive to feature selection variations and illumination conditions (angle of incidence and intensity) for calculating focus measures, making autofocusing-based contact detection unreliable. More importantly, the depth of field of microscope objectives is on the order of a few microns to tens of microns, which makes images of two objects with distinctly different world coordinates reveal sharpness over a distance of micrometers. Thus, autofocusing-based methods are not capable of accurately bringing the micropipette tip and the glass slide surface to an exact co-plane.

This paper reports on a computer vision-based method that addresses the detection of contact between an end-effector and a target surface. The fundamental rationale is based on the experimental observation that when contact is established, further vertical motion of the end-effector (flexible or stiff) produces horizontal motion in the image plane. As shown in Figure 2, upon contact, further motion of the end-effector along the vertical direction (Z) is translated to horizontal motion along the X direction and reflects itself in the image plane. This general observation is not limited to contact between a micropipette tip and a glass slide surface although the contact between a micropipette tip and a glass slide is used as an example to illustrate the detection method, as long as the target surface roughness is not sufficiently high to significantly alter the horizontal motion of the end-effector or obscure the identification and tracking of the end-effector.

The paper is structured as follows. A computer-vision based contact detection analysis is given in Section 2. The method

for determining the region of interest (i.e., tip area) is described in Section 3. Section 4 presents the methodology of contact detection using a pixel-accuracy method and a sub-pixel-accuracy method. Experimental results are presented in Section 5.

2. Contact Detection Analysis

Figure 3 shows a schematic consisting of an image plane, microscope objective, the end-effector (e.g., micropipette tip), and the target surface. Throughout the paper, the world frame is denoted by X - Y - Z , and image plane by x - y . When the tip is controlled by a microrobot to move downwards at a constant speed, the initial tip position, position before contact, exact contact position, and position after contact are denoted as Position 1, 2, 3, and 4 in the world frame and $1'$, $2'$, $3'$, and $4'$ in the image plane. '0' is taken as the origin of the image plane, and 'O' the origin of the world frame.

Denote the distance between the tip at initial Position 1 and the target surface by h , the distance between the tip at Position 1 and the objective by u , and the distance between the image plane and the objective by v . The horizontal distance between the tip and the optical axis is denoted by X_0 . In practice, the target surface is first brought into focus before contact detection is conducted; however, the initial position of the end-effector does not need to lie within the depth of field.

Before contact is established, similarity of triangles gives

$$\frac{x}{X_0} = \frac{v}{u + Z} \quad (1)$$

Differentiating both sides yields

$$dx = -\frac{v \cdot X_0}{u^2} dZ \quad (2)$$

which implies that prior to contact, the x coordinate values of the tip **decrease** in proportion to downward displacements along the Z direction in the world frame.

Similarly, after contact is established,

$$dx = \frac{v \cdot \tan(\theta/2)}{u} dZ \quad (3)$$

implying that after contact, the x coordinate values of the tip **increase** in proportion to downward displacements along the Z direction in the world frame.

In summary, the brief analysis demonstrates that the x -coordinate values of the micropipette tip in the image plane decrease before contact and then increase after contact. When the micropipette tip reaches the minimal x -coordinate value in the image plane, initial contact occurs between the micropipette tip and the target surface. Thus, the relative vertical position between the end-effector and target surface is determined by monitoring the pattern change in the x -coordinate values of the end-effector, differing this contact detection method from autofocusing-based techniques. See also Extension 1.

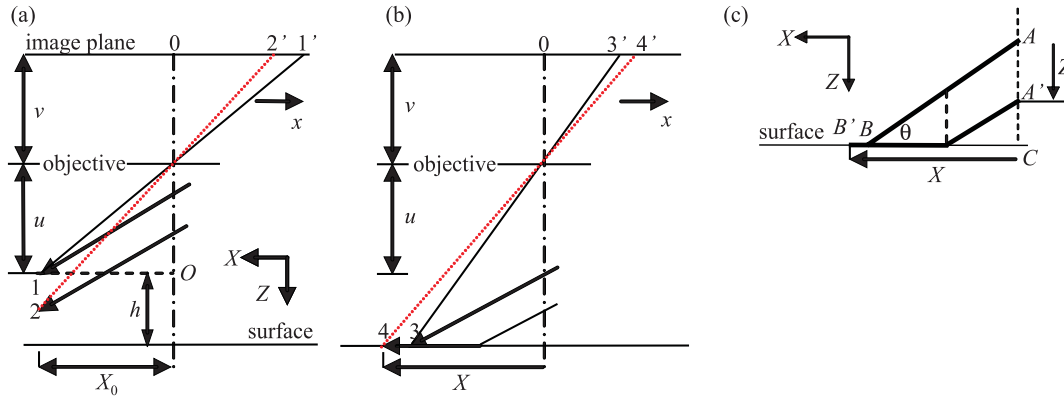


Fig. 3. Contact detection analysis. (a) Before contact. (b) After contact. (c) Horizontal sliding after contact.

Table 1. Preprocessing Steps for Tip Area Identification

Step #	Processing
1	Contrast stretching, mapping the gray levels from the original range to a full range of [0, 255]
2	Adaptive thresholding
3	Morphological operations: erosion and dilation to remove small areas regarded as noises that produce many separate artificial objects, and to connect segments that originally are of one object

3. Tip Area Identification

In order to identify the region of interest (ROI) surrounding the micropipette tip for subsequent contact detection that will be described in Section 4, an identification algorithm is developed. The algorithm distinguishes a moving object by subtracting the unchanged background from each frame of image. The micropipette, not required to be in focus, is moved by a microrobot horizontally (Y) at a constant speed without Z motion, producing motion along the y direction in the image plane (Figure 4). In practice, the Z -axis of the microrobot is aligned parallel to the optical axis by adjusting the microrobot base (X - Y); and the image plane x - y is aligned parallel to the X - Y plane by rotating the camera adaptor. Full-frame images (640×480) are processed in real time (30 Hz) for locating the ROI that contains the micropipette tip.

Denote image frames by $I(x, y, t)$, where $t = 0, 1, 2, \dots$. Each image frame is first convolved with a low-pass Gaussian filter for noise suppression. The resulting image is denoted by $F(x, y, t)$. For each frame in an image sequence, its gray-level difference with respect to the very first frame ($t = 0$) is

$$D(x, y, t) = F(x, y, t) - F(x, y, 0) \quad (4)$$

Table 1 summarizes preprocessing steps that are applied to image $D(x, y, t)$. Resulting images are shown in Figure 5.

As the micropipette continues to move along the Y direction, the number of connected entities represented by bound-

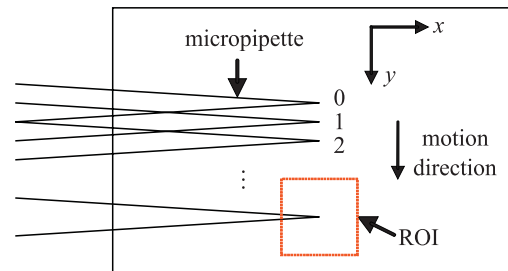


Fig. 4. Micropipette moves along the y direction in the image plane (Y in the world frame) for tip area identification.

ary chain codes (Castleman 1996) in images decreases dramatically. When the number of entities decreases by 90% in two successive frames, the entity with the maximum area is recognized as the micropipette. The tip is located on the rightmost end of the micropipette in this example. A ROI (e.g., 100×80) shown in Figure 5(h) around the tip is then chosen for subsequent contact detection. Typically, the ROI is found at Frame 4 ($t = 4$).

After the determination of ROI, the micropipette stops moving along the Y direction. It is then controlled to move along the downward direction (Z) at a constant speed to establish contact with the surface. In the subsequent contact detection process described in Section 4, image processing is only conducted inside the ROI to alleviate computation complexity and allow real-time performance.

Table 2. Processing Steps for Contact Detection

Step #	Processing
1	Gaussian low-pass filtering
2	Adaptive thresholding with the Otsu method
3	Morphological operation (erosion and dilation)
4	Tip's x coordinate in image update
5	If current x coordinate exceeds the minimal value by 6 pixels, moving the micropipette back to the Z position of the contact point corresponding to the minimal value. Otherwise, update the minimal x value and go back to Step 1

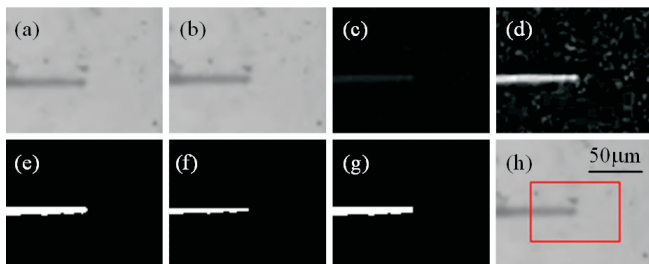


Fig. 5. Sequence for identifying the tip (i.e., determination of ROI). (a) Frame 0. (b) Frame 4. (c) Differentiation image between (b) and (a). (d) Image after contrast stretching of (c). (e) Thresholded image of (d). (f) Erosion image of (e). (g) Dilation image of (f). (h) ROI found at Frame 4.

4. Contact Detection

As shown in Figure 2, upon contact, the tip is located at a . After the establishment of contact, the tip slides horizontally from location a to b on the surface. Contact detection leverages such changes in the x coordinate in the image plane. As the brief analysis in Section 2 shows, physical contact occurs when the tip reaches its minimal x -coordinate value. After the identification of ROI, the micropipette moves downwards at a constant speed until its x -coordinate surpasses the minimal value by a few pixels (e.g., 6 pixels). Surpassing more pixels represents larger micropipette tip deformations that can lead to micropipette breakage, but constitutes less of a concern for stiff end-effectors such as micro probes for MEMS and IC testing. During this process, the precise Z positions of the microrobot corresponding to each frame of image are recorded. Thus, the microrobot can precisely bring the micropipette tip back to the exact contact position after the completion of contact detection.

The processing sequence for contact detection is described in Table 2. Note that ROIs of images $I(x, y, t)$ rather than the differentiation images $D(x, y, t)$ are processed for all the five processing steps, including the first three steps of preprocessing. In Step 4, the micropipette tip is identified by searching for the object with the maximum area in the ROI. Inside

the ROI (step 5), tasks include: (1) to determine the tip's x -coordinate value using either a pixel-accuracy method or a sub-pixel-accuracy method that will be discussed in Section 4.1 and Section 4.2; (2) to compare the current x -coordinate value with the current minimal value and update the minimal value, if needed.

4.1. Tracking Tip with Pixel Accuracy

A representative experimental curve of micropipette tip's x coordinate changes versus frame indices is shown in Figure 6. Point 1 corresponds to the first frame in the valley. Point 2 is one pixel above the valley. Similarly, Point 6 is five pixels above the valley. The valley lasts a number of frames between Point 1 and Point 2. Within this valley band lies the exact contact point that can be determined by interpreting (3).

(3) reveals that after contact, each increment of one pixel in the x coordinate corresponds to an equal displacement along the Z direction in the world frame. The frame index for the contact point (Point P in Figure 6), f_P can be obtained as $f_2 - N$, where f_2 is the frame index for Point 2, and N is the number of frames between Point 2 and Point 3. However, as the number of frames between Point 2 and Point 3 and the one between Point 3 and Point 4 are not strictly equal, numbers of frames per pixel step are averaged to reduce the error of locating f_P .

$$f_P = f_2 - (f_6 - f_2)/4 \quad (5)$$

where f_6 is the frame index for Point 6. Based on the determined f_P , the microrobot brings the micropipette tip back to the initial contact position according to the recorded positions that correspond to each frame of image.

4.2. Tracking Tip with Sub-Pixel Accuracy

The accuracy using (5) to determine the contact point is limited due to the fact that numbers of frames between Point 2 and 3... and between Point 5 and 6 are slightly different. In order to further improve the detection accuracy, an edge detection algorithm based on moment invariance (Kim et al. 1999)

is employed to track the micropipette tip with a sub-pixel accuracy.

A step edge in the absence of noise is characterized by a set of pixels having gray levels L_i ($i = 0, 1, 2, \dots, n - 1$) that are either monotonically non-decreasing or non-increasing. As shown in Figure 7, an ideal edge is a sequence of pixels with one gray level h_1 , followed by a sequence of pixels with another gray level h_2 , where k denotes the edge location to be determined.

The first three moments of the input data are

$$\bar{m}_j = \frac{1}{n} \sum_{i=0}^{n-1} (L_i)^j \quad j = 1, 2, 3 \quad (6)$$

The solutions of the edge are

$$h_1 = \bar{m}_1 - d\sqrt{p_2/p_1} \quad (7)$$

$$h_2 = \bar{m}_1 + d\sqrt{p_1/p_2} \quad (8)$$

$$p_1 = [1 + s\sqrt{1/(4 + s^2)}]/2 \quad (9)$$

where

$$s = (\bar{m}_3 + 2\bar{m}_1^3 - 3\bar{m}_1 \cdot \bar{m}_2)/d^3$$

$$d = \sqrt{\bar{m}_2 - \bar{m}_1^2}$$

$$p_1 + p_2 = 1$$

Thus, the edge location is determined as

$$k = p_1 \cdot n. \quad (10)$$

To obtain the x coordinate of the tip using the sub-pixel-accuracy method, a certain number (e.g., $n = 11$) of pixels along the x -axis are selected around the tip located with the pixel-accuracy method. Let the x coordinate of the tip located with the pixel-accuracy method be k_0 . Pixels with x coordinates $k_0 - 5, k_0 - 4, k_0 - 3, \dots, k_0 + 3, k_0 + 4,$ and $k_0 + 5$ are used to calculate the x coordinate of the tip with sub-pixel accuracy according to (6)–(10). In Figure 6, the dashed curve shows the x coordinate values of the micropipette tip obtained via the sub-pixel-accuracy method.

The curve, however, is not smooth due to image noise. Around the valley point of this V-shaped, dashed curve also exist false spikes that affect the accuracy of contact point determination. Thus, to reduce the error, the original curve is divided into two parts from the valley point that has the minimal x coordinate of the tip, each side fitted into a straight line using the Huber method (Huber 1981), which is a weighted linear least squares method. Let r_i represent the distance between the i th data point and the fitted line. $\rho(r_i)$ is a distance function

$$\rho(r_i) = \begin{cases} r_i^2/2 & \text{if } r_i < c \\ c \cdot (r_i - c/2) & \text{else} \end{cases} \quad (11)$$

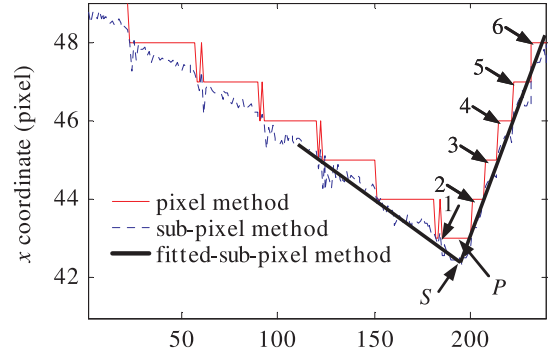


Fig. 6. Tip x -coordinate versus frame index when moving downwards along Z in world frame. (speed: $14 \mu\text{m/s}$, mag.: $9\times$)

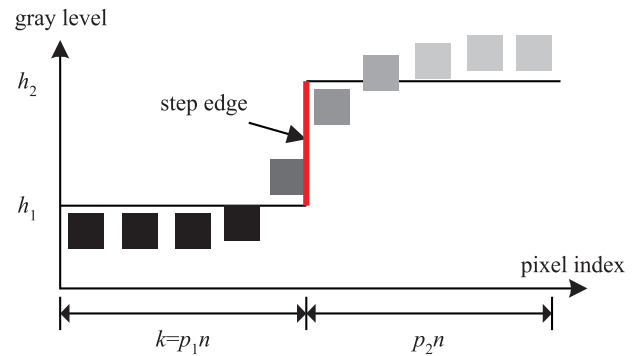


Fig. 7. Edge detection with moment invariance. Each square represents a pixel with different gray levels.

The line is obtained by minimizing

$$\varepsilon = \sum_i \rho(r_i) \quad (12)$$

The constant c limits the influence of outliers and was chosen to be 0.05 under the experimental conditions. The intersection point of the two fitted lines is taken as the contact point (Point S in Figure 6).

5. Experimental Results

5.1. Experimental Setup

The system, shown in Figure 8, consists of a stage holding a glass slide, an optical microscope (Olympus SZX12) with a CMOS digital camera (Basler A601f), and a three-degrees-of-freedom microrobot with a travel of 25 mm and a $0.04 \mu\text{m}$ positioning resolution along each axis (MP-285, SUTTER). The microrobot is controlled via a motion control board (NI PCI-6259), carrying a glass micropipette (TW120F-4) with a $5 \mu\text{m}$

Table 3. Effect of Illumination Intensity (speed: 58 $\mu\text{m/s}$, mag.: 9 \times)

Intensity	Low		Medium		High	
	pix-accuracy	sub-pixel-accuracy	pix-accuracy	sub-pixel-accuracy	pix-accuracy	sub-pixel-accuracy
m (μm)	7410.1	7410.8	7410.8	7411.4	7410.4	7411.0
σ (μm)	1.6	1.3	1.2	0.9	1.3	0.6

Table 4. Effect of Microrobot Speed (Mag.: 9 \times)

Speed	14($\mu\text{m/s}$)		58($\mu\text{m/s}$)		380($\mu\text{m/s}$)	
	pix-accuracy	sub-pixel-accuracy	pix-accuracy	sub-pixel-accuracy	pix-accuracy	sub-pixel-accuracy
m (μm)	7410.2	7410.7	7410.8	7411.4	7419.9	7422.6
σ (μm)	1.4	1.3	1.2	0.9	7.9	6.4

Table 5. Effect of Magnifications (speed: 58 $\mu\text{m/s}$)

Mag.	1.25 \times		2.5 \times		5 \times		9 \times	
	pix-accuracy	sub-pixel	pix-accuracy	sub-pixel	pix-accuracy	sub-pixel	pix-accuracy	sub-pixel
m (μm)	7398.4	7409.2	7402.8	7410.8	7407.3	7411.0	7410.8	7411.4
σ (μm)	3.6	2.7	2.4	1.6	2.1	1.8	1.2	0.9

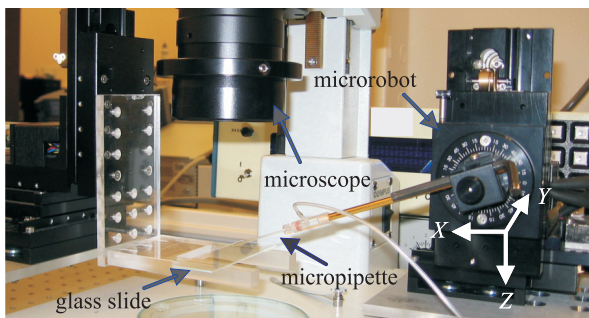


Fig. 8. System setup used to test contact detection during microrobotic cell manipulation.

tip and tilting angle from the target surface of the glass slide $\theta = 20^\circ$. The system setup is mounted on a vibration isolation table.

5.2. Performance Evaluation

In the beginning of experiments, the glass slide serving as the target surface was brought in focus and kept unchanged thereafter. In terms of microrobot motion, the micropipette was first moved laterally for ROI determination and then, moved vertically to establish contact. In order to evaluate the performance of the computer vision-based contact detection method,

effects of variations in illumination intensity, microrobot motion speed in lowering the micropipette, and magnifications of the microscope on detection accuracy were experimentally investigated. Experiments were repeated 50 times for studying each effect, amounting to a total of 1000 experimental trials. Tables 3, 4, and 5 summarize contact detection results in terms of the mean (m) and standard deviation (σ).

First, the experimental results demonstrate that the sub-pixel-accuracy method provides more accurate detection results than the pixel-accuracy method. This is attributed to the fact that the sub-pixel-accuracy method uses more data points for line fitting and thus, locates the contact point more accurately. Secondly, both algorithms are not significantly affected by illumination intensity variations (Table 3). Thirdly, a very high motion speed produces a high standard deviation (Table 4). Finally, under a higher magnification, both the pixel-accuracy and sub-pixel-accuracy methods provide higher detection accuracy (Table 5).

The presented contact detection method was proven robust. In all the 1000 experimental trials, contact detection was achieved without the occurrence of micropipette tip breakage using both the pixel-accuracy method and sub-pixel-accuracy method. For the majority of the trials, the standard deviation of contact detection is smaller than 2 μm . When the motion speed was high (380 $\mu\text{m/s}$), the largest standard deviation occurred (7.9 μm for the pixel-accuracy method; 6.4 μm for the sub-pixel-accuracy method). This high motion speed produced a large vertical displacement (12.7 μm) along the Z direction be-

Table 6. Deformation versus Force along the Z Direction

Force (μN)	0.05	0.1	0.2	0.5	1.0
Max. tip displacement (μm)	0.12	0.24	0.48	1.19	2.38

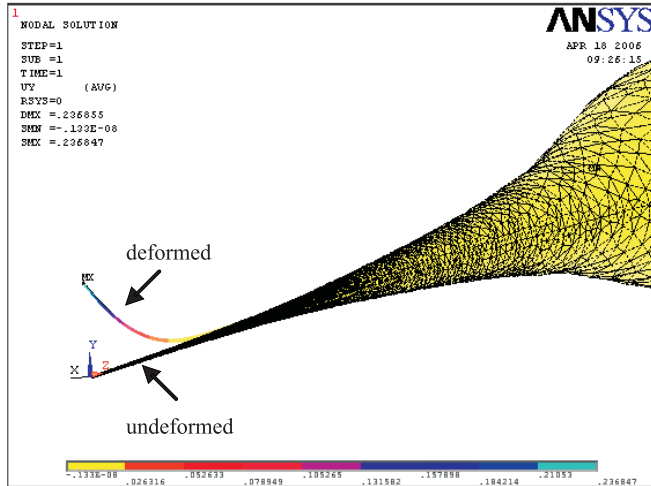


Fig. 9. Finite element structural simulation (tip deflection vs. applied force) of micropipette contact with a solid substrate. Unit is μm for deformations. Deflection in the figure is exaggerated for visualization purposes.

tween two successive frames of images, causing a large contact detection deviation. Additionally, an extremely high motion speed could cause damage to the delicate end-effector and/or target surface resulting from excessive impact.

5.3. Validation

5.3.1. Finite Element Simulation

A 3-D finite element model was constructed according to the geometries of the micropipette used in the experiments. Structural simulation was conducted using ANSYS[®], in which the material parameters of glass (Young's modulus of 6.5 GPa, Poisson ratio of 0.2) for the micropipette were used. The relationship between contact forces and micropipette tip deformations along the Z direction was established. The simulation results are summarized in Table 6. A larger contact force results in a larger structural deformation (Figure 9). Corresponding to a contact force of 0.1 μN , the micropipette tip deforms by 0.24 μm .

5.3.2. Calibration Experiments

In order to verify the accuracy of the contact points determined by the computer vision-based detection method, the

Table 7. Z Readings for Contact Points (μm)

Trial group #	Balance-measured position	Pixel-accuracy method	Sub-pixel-accuracy method
1	2961.0	2958.2	2961.4
2	3031.0	3029.4	3031.2

glass slide was placed on an analytical balance for detecting contact forces (XP205, Mettler Toledo, resolution 0.1 μN). In the validation experiments, the micropipette was controlled by the microrobot to move downwards at a speed of 14 $\mu\text{m/s}$. A magnification of 3.2 \times was used. Using the computer vision-based contact detection method, 100 experimental trials were conducted (50 using the pixel-accuracy methods; 50 using the sub-pixel-accuracy method) in each trial group (two trial groups amounting to 200 trials in total). The mean values of the located contact points are summarized in Table 7, where the 'real' contact positions were determined by reading a contact force change of the balance from zero to 0.01 mg (0.1 μN). Comparing the balance measured results with the results from the computer vision-based contact detection method, an accuracy down to 0.2 μm was achieved (i.e., difference between 'real' contact position and computer vision detected position).

6. Conclusion

This paper presented a computer-vision based method for visually detecting the contact between an end-effector and a target surface under an optical microscope without using additional proximity or force/touch sensors. The rationale behind the algorithm is based on the fact that after the establishment of a contact, further vertical motion in the world frame induces horizontal motion in the image plane. Without requiring the end-effector to be in focus, detection starts with the determination of a region of interest, and then further detects the contact point using either a pixel-accuracy or a sub-pixel-accuracy method. Experiments demonstrated that the computer vision-based method is capable of achieving contact detection between a micropipette tip and a glass slide surface with an accuracy of 0.2 μm . The robustness of the contact detection method was experimentally demonstrated through varying several factors including illumination intensity, magnification, and microrobot motion speed. The presented contact detection method is applicable to many microrobotic and nanorobotic manipulation scenarios, in which flexible or stiff end-effectors are operated under an optical or electron microscope.

Appendix: Index to Multimedia Extensions

The multimedia extension page is found at <http://www.ijrr.org>.

Table of Multimedia Extensions

Extension	Type	Description
1	Video	After the establishment of contact in the world frame, further vertical motion of the end-effector induces horizontal motion in the image plane. Detection of the contact between the end-effector and target surface is equivalent to locating the global minimum of x coordinates of the end-effector in the image plane with either a pixel resolution or sub-pixel resolution method.

References

- Arai, F., Motoo, K., Kwon, P. G. R., Fukuda, T., Ichikawa, A., and Katsuragi, T. (2003). Novel touch sensor with piezoelectric thin film for microbial separation, *Proceedings of IEEE International Conference on Robotics and Automation*, Taipei, September, pp. 306–311.
- Castleman, K. R. (1996). *Digital Image Processing*. Prentice Hall, Englewood Cliffs, NJ, pp. 479–480.
- Fukuda, T., Sato, H., Arai, F., Iwata, H., and Itoigawa, K. (1998). Parallel beam micro sensor/actuator unit using PZT thin films and application examples. *Proceedings of IEEE International Conference on Robotics and Automation*, Leuven, Belgium, May, pp. 1498–1503.
- Geusebroek, J. M., Cornelissen, F., Smeulden, A. W. M., and Gee, H. (2000). Robust autofocusing in microscopy, *Cytometry*, **36**(1): 1–9.
- Haitjema, H., Pril, W., and Schellekens, P. H. J. (2001). A silicon-etched probe for 3-D coordinate measurements with an uncertainty below 0.1 μm . *IEEE Transactions on Instrumentation and Measurement*, **50**(6): 1519–1523.
- Hatzivasilou, F. V. and Tzafestas, S. G. (1994). Analysis and design of a new piezoresistive tactile sensor system for robotic applications. *Journal of Intelligent and Robotic Systems*, **10**(3): 243–256.
- Huber, P. J. (1981). *Robust Statistics*. Wiley, New York.
- Junno, T., Deppert, K., Montelius, L., and Samuelson, L. (1995). Controlled manipulation of nanoparticles with an atomic force microscopy. *Applied Physics Letters*, **66**(26): 3627–3629.
- Kanda, T., Morita, T., Kurosawa, M. K., and Higuchi, T. (1999). A rod-shaped vibro touch sensor using PZT thin film *IEEE Transactions on Ultrasonics, Ferroelectrics and Frequency Control*, **46**(4): 875–882.
- Kim, T. H., Moon, Y. S., and Han, C. S. (1999). An efficient method of estimating edge locations with subpixel accuracy in noisy images, *IEEE Region 10 Conference, TENCN*, Cheju, Korea, September, pp. 589–592.
- Lee, H., Purdon, A. M., and Westervelt, R. M. (2004). Micromanipulation of biological systems with microelectromagnets. *IEEE Transactions on Magnetism*, **40**(4): 2991–2993.
- Li, Y. F. (1996). A sensor-based robot transition control strategy. *International Journal of Robotics Research*, **15**(2): 128–136.
- Ramachandran, T. R., Baur, C., Bugacov, A., Koel, B. E., Requicha, A., and Gazez, C. (1998). Direct and controlled manipulation of nanometer-sized particles using the non-contact atomic force microscope. *Nanotechnology*, **9**(3): 237–245.
- Shen, Y. T., Xi, N., Lai, K. W. C., and Li, W. J. (2004). A novel PVDF microforce/force rate sensor for practical applications in micromanipulation. *Sensor Review*, **24**(3): 274–283.
- Sitti, M. and Hashimoto, H. (2000). Two-dimensional fine particle positioning under optical microscope using a piezoresistive cantilever as a manipulator. *Journal of Micro-mechatronics*, **1**(1): 25–48.
- Subbarao, M. and Tyan, J. K. (1998). Selecting the optimal focus measure for autofocusing and depth-from-focus. *IEEE Transactions on Pattern Analysis and Machine Intelligence*, **20**(8): 864–870.
- Sun, Y. and Nelson, B. J. (2002). Biological cell injection using an autonomous microrobotic system, *International Journal of Robotics Research*, **21**(10–11): 861–868.
- Sun, Y., Duthaler, S., and Nelson, B. J. (2004). Autofocusing in computer microscopy: selecting the optimal focus algorithm. *Microscopy Research and Technique*, **65**(3): 139–149.
- Trummer, G., Kurzals, C., Gehring, R., and Leistner, D. (2004). Next-generation proximity and position sensors. *Sensors*, **21**(3): 14–21.
- Vikramaditya, B. and Nelson, B. J. (1999). Visually servoed micropositioning for robotic micromanipulation. *Micro-computer Applications*, **18**(1): 23–31.